Check for updates

Expression patterns of platinum resistance-related genes in lung adenocarcinoma and related clinical value models

Zhe Wang[1†], Lin Mu[2†], He Feng[3†], Jialin Yao[1], Qin Wang[1], Wenxiao Yang[1], Huiling Zhou[1], Qinglin Li[3]* and Ling Xu[1]*

[1]Department of Oncology, Yueyang Hospital of Integrated Traditional Chinese and Western Medicine, Shanghai University of Traditional Chinese Medicine, Shanghai, China, [2]Department of Ophthalmology, Longhua Hospital Shanghai University of Traditional Chinese Medicine, Shanghai, China, [3]Cancer Hospital of the University of Chinese Academy of Sciences (Zhejiang Cancer Hospital), Zhejiang, China

The purpose of this study was to explore platinum resistance-related biomarkers and mechanisms in lung adenocarcinoma. Through the analysis of gene expression data of lung adenocarcinoma patients and normal patients from The Cancer Genome Atlas, Gene Expression Omnibus database, and A database of genes related to platinum resistance, platinum resistance genes in lung adenocarcinoma and platinum resistance-related differentially expressed genes were obtained. After screening by a statistical significance threshold, a total of 252 genes were defined as platinum resistance genes with significant differential expression, of which 161 were up-regulated and 91 were down-regulated. The enrichment results of up-regulated gene Gene Ontology (GO) showed that TOP3 entries related to biological processes (BP) were double-strand break repair, DNA recombination, DNA replication, the down-regulated gene GO enriches the TOP3 items about biological processes (BP) as a response to lipopolysaccharide, muscle cell proliferation, response to molecule of bacterial origin. Gene Set Enrichment Analysis showed that the top three were e2f targets, g2m checkpoint, and rgf beta signaling. A prognostic model based on non-negative matrix factorization classification showed the characteristics of high- and low-risk groups. The prognostic model established by least absolute shrinkage and selection operator regression and risk factor analysis showed that genes such as HOXB7, NT5E, and KRT18 were positively correlated with risk score. By analyzing the differences in m6A regulatory factors between high- and low-risk groups, it was found that FTO, GPM6A, METTL3, and YTHDC2 were higher in the low-risk group, while HNRNPA2B1, HNRNPC, TGF2BP1, IGF2BP2, IGF2BP3, and RBM15B were higher in the high-risk group. Immune infiltration and drug sensitivity analysis also showed the gene characteristics of the platinum-resistant population in lung adenocarcinoma. ceRNA analysis showed that has-miR-374a-5p and RP6-24A23.7 were lower in the tumor expression group, and that the survival of the low expression group was worse than that of the high expression group. In conclusion, the results of this study show that platinum resistance-related differentially expressed genes in lung adenocarcinoma are mainly concentrated in biological processes such as DNA recombination and response to lipopolysaccharide. The validation set proved that the high-risk group of our

prognostic model had poor survival. M6A regulatory factor analysis, immune infiltration, and drug sensitivity analysis all showed differences between high and low-risk groups. ceRNA analysis showed that has-miR-374a-5p and RP6-24A23.7 could be protective factors. Further exploration of the potential impact of these genes on the risk and prognosis of drug-resistant patients with lung adenocarcinoma would provide theoretical support for future research.

1 Introduction

Globally, the mortality rate of lung cancer is the highest among all tumors (Xia et al., 2022). Non-small cell lung cancer (NSCLC), which accounts for 80% of all lung cancer cases (Miller et al., 2016), can be divided into three main pathological subtypes: adenocarcinoma (40%), squamous cell carcinoma (30%), and large cell carcinoma (15%) (Ruiz-Cordero and Devine, 2020; Travis et al., 2016). The standard first-line treatment is still platinum-based combined chemotherapy (Scagliotti et al., 2002; Schiller et al., 2002). Although chemotherapy can bring benefits to lung adenocarcinoma (LUAD) patients, the median progression-free survival time is only 5.5 months (West et al., 2019), and drug resistance is inevitable. Although many studies have explored the mechanism of platinum drug resistance, there is still no clear mechanism or targets of platinum drug resistance, and few research results can be used in clinical application. Therefore, we aimed to explore the potential biomarkers and mechanisms of platinum-based drug resistance genes in LUAD, establish a prognostic model, and conduct related research on clinical prognosis and risk.

The rapid development of immunotherapy over the last decade has led to the improvement of immune checkpoint inhibitors, which has improved the clinical outcomes of some patients with advanced cancer and changed the treatment status of NSCLC (Osmani et al., 2018; Queirolo and Spagnolo, 2017). Therefore, attention has been paid to immune cell infiltration, the role of immune infiltration in the occurrence, development, and prognosis of platinum-based LUAD, prognostic information, and predicting the efficacy of immunotherapy. Drug sensitivity analysis can also provide guidance for follow-up treatment of platinum-resistant patients with LUAD. Several studies have shown that mRNA methylation plays an important role in the occurrence and development of some cancers (e.g., glioblastoma, renal clear cell carcinoma, and pancreatic cancer) (Cui et al., 2017; Du et al., 2020; Geng et al., 2020; Lan et al., 2019; Wang et al., 2020). These studies indicated that the development of tumors may be related to the expression of key genes related to the function of the m6A regulator. However, there is no research on the m6A methylation regulatory factor with respect to platinum drug resistance in LUAD.

In this study, we aimed to identify the characteristics of platinum drug resistance genes in LUAD, and explore the characteristics of patients after drug resistance, to pave the way for further study of drug resistance mechanisms. We first explored the expression patterns of platinum-resistant genes related to LUAD in The Cancer Genome Atlas (TCGA), Gene Expression Omnibus (GEO), and A database of genes related to platinum resistance. Functional annotations and channel analysis of different platinum resistance genes were performed through Gene Ontology (GO), Kyoto Encyclopedia of Genes and Genomes (KEGG) and Gene Set Enrichment Analysis (GSEA). Subsequently, we evaluated the ability to transform into clinical applications through non-negative matrix factorization (NMF) cluster analysis and the establishment of a prognosis model. Immune infiltration and drug sensitivity analyses were used to evaluate the possible applicability of patients with LUAD platinum resistance to other clinical treatments. The results of this study provide guidance for the development of clinical drugs for platinum-resistant patients with LUAD. Workflow is shown in Figure 1.

2 Materials and methods

2.1 Expression datasets and bioinformatic analysis

2.1.1 Data and preprocessing

We downloaded the gene expression profile, miRNA expression profile, and clinical information data of LUAD from the TCGA database (n = 585) (https://tcga-data.nci.nih.gov/tcga/). A total of 912 genes related to platinum resistance were downloaded from A database of genes related to platinum resistance (http://ptrc-ddr.cptac-data-view.org). Finally, expression data and clinical information of 116 LUAD samples (data number GSE26939) were downloaded from the GEO database (https://www.ncbi.nlm.nih.gov/geo/query/acc.cgi?acc=GSE26939) for use as the verification dataset.

2.1.2 Differentially expressed gene (DEG) analysis

We analyzed the differences in gene expression between cancer and normal patients using the R package DESeq2 (v1.

FIGURE 1
Workflow (Modify database name).
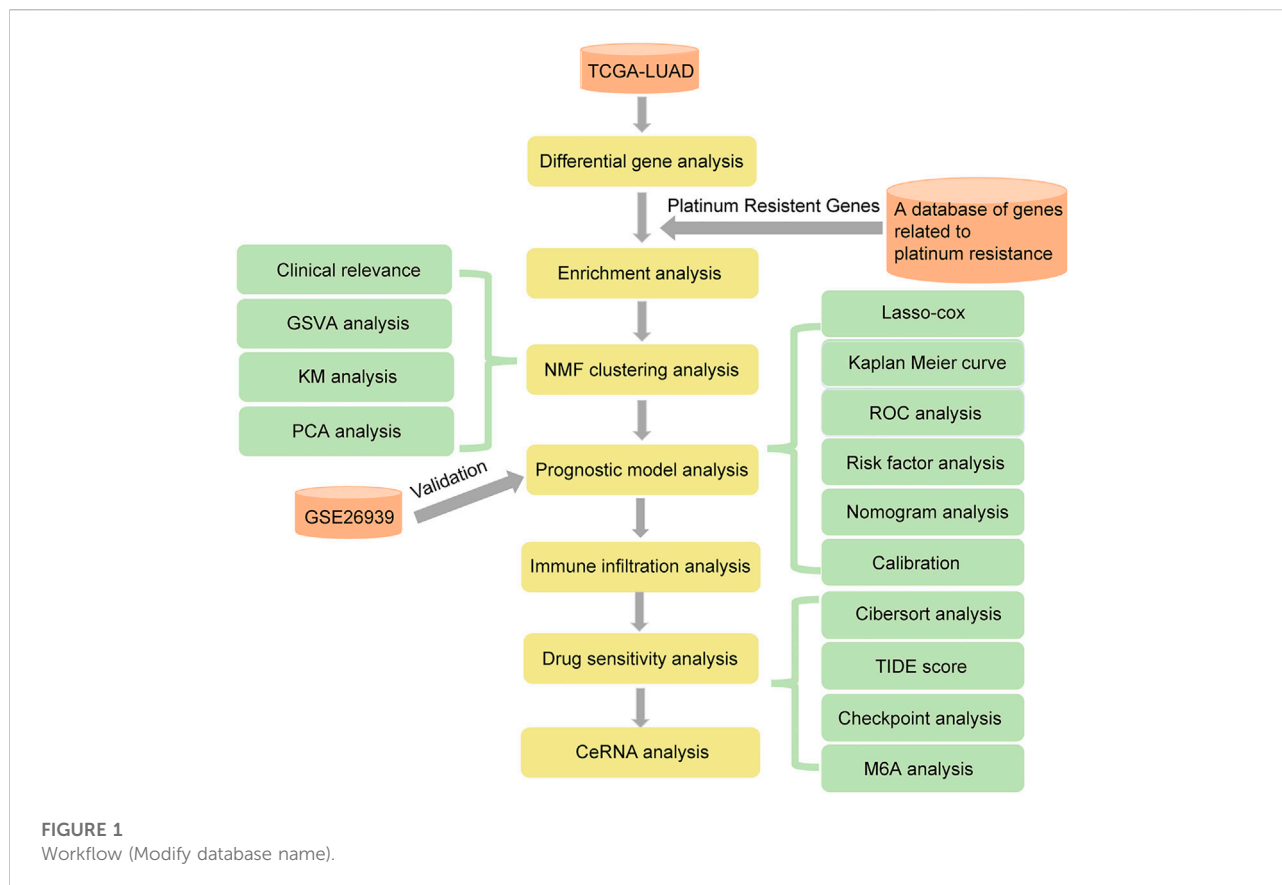
32.0) (Love et al., 2014). We set | log2fold change | (| log2fc |) ≥ 1 and adjust p value <0.05 as the threshold of differential genes; log2fc ≥ 1 and adjust p value <0.05 gene was used to identify upregulated genes, while log2fc ≤ −1 and adjust p value ≤0.05 were used to identify downregulated genes. Cisplatin-based chemotherapy is a common method to treat LUAD. However, after developing resistance to cis-diammine di chloroplatinum (CDDP), a considerable number of patients' tumors recurred. Therefore, screening patients with primary resistance to cisplatin in the LUAD population can maximize the clinical benefit. To further reveal the biological functions affected by the DEGs related to platinum resistance, the intersection of platinum resistance genes and DEGs was defined as PRR-DEGs. We used a volcano map and heatmap to visualize platinum resistance genes with significant differential expression. The volcano map was drawn using the R package ggplot2 (v3.3.5), the heat diagram was drawn using the R package pheatmap (v1.0.12) (Figure 2A). The detailed information is shown in Supplementary Table S1.
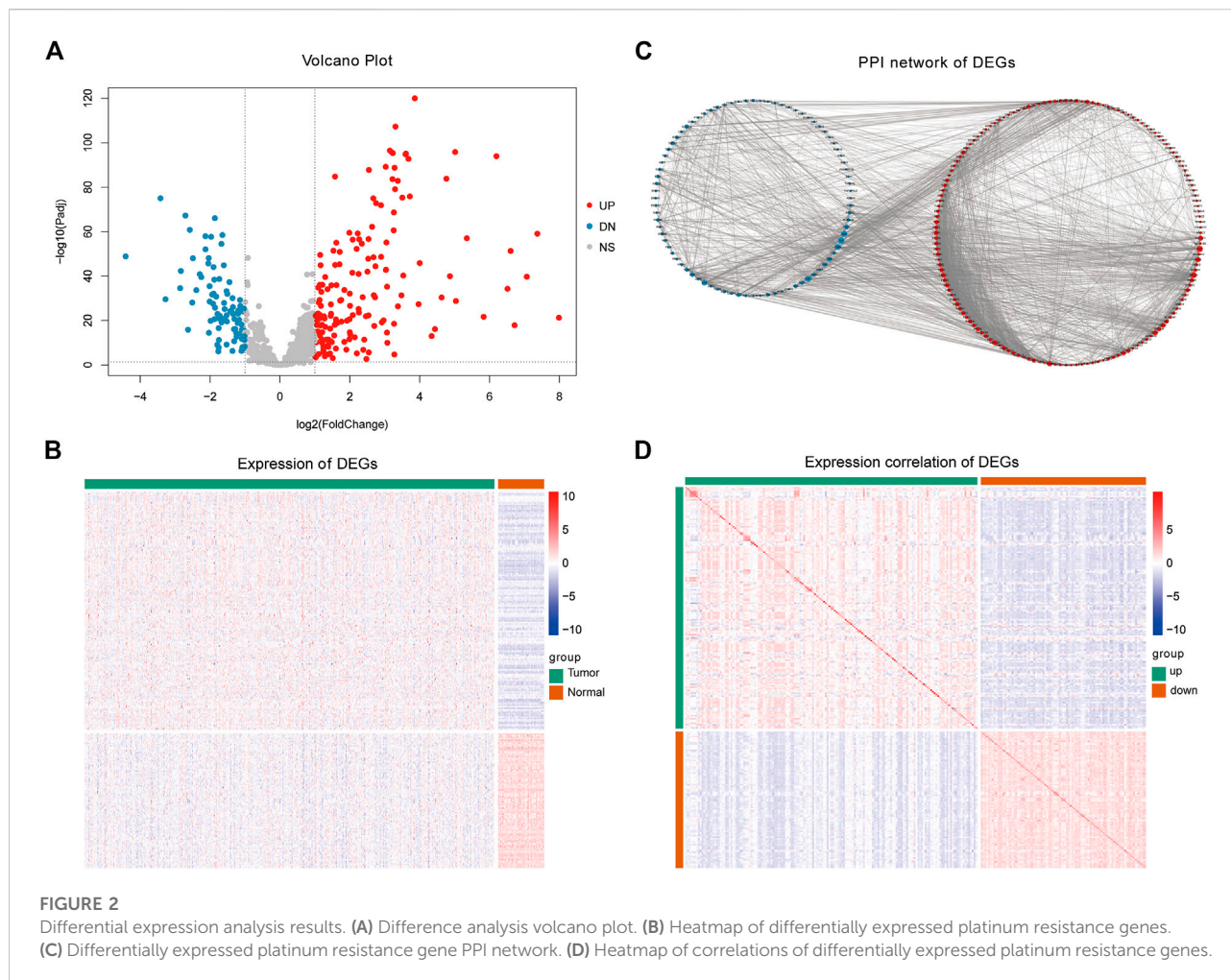
The expression of different genes is interrelated, especially among genes that regulate the same biological process. Therefore, to reveal the relationships between the PRR-DEGs, a protein–protein interaction network (PPI) was constructed

based on the platinum resistance-DEGs. Using the String database (https://www.string-db.org) (Mering, 2003), the above genes were used as input, and the default confidence threshold was 0.4 (Figure 2B). The PPI network was constructed, and the visualization was carried out using the Cytoscape (v3.8.2) (Shannon et al., 2003) software. The expression correlation of PRR-DEGs was calculated and visualized using a nomogram.

2.1.3 Functional enrichment analysis

GO (Http://geneontology.org/) is a common method for large-scale functional enrichment of genes in different dimensions and levels. It is generally carried out from three levels: biological process (BP), molecular function (MF), and cellular component (CC) (Harris et al., 2004). The R package cluster Profiler (v4.0.5) (Wu et al., 2021) was used for GO functional annotation analysis of all the genes with significantly different expression levels to identify the biological processes and pathways with significant enrichment. The enrichment results were visualized using the R package GOplot (v1.0.2) (Walter et al., 2015). The significance threshold of enrichment analysis was set as adjust p value ≤0.05 (Figures 3A,C).

KEGG (https://www.kegg.jp/) is a utility database resource for understanding advanced functions and biological systems

FIGURE 2
Differential expression analysis results. **(A)** Difference analysis volcano plot. **(B)** Heatmap of differentially expressed platinum resistance genes.
(C) Differentially expressed platinum resistance gene PPI network. **(D)** Heatmap of correlations of differentially expressed platinum resistance genes.
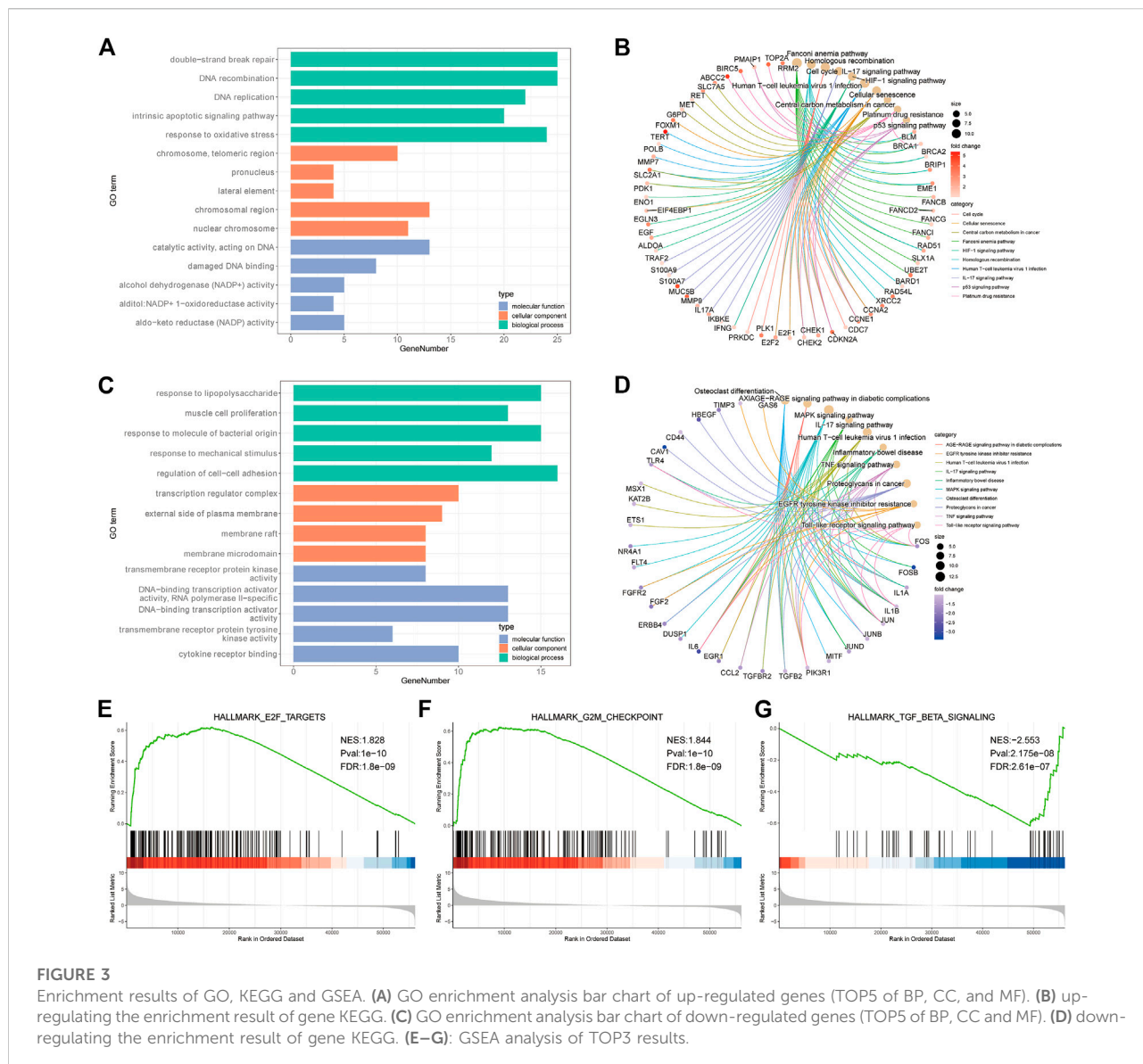
(such as cells, organisms and ecosystems), genome sequencing and other high-throughput experimental techniques generated from molecular level information, especially large molecular data sets. It was established in 1995 by Kanehisa Laboratory of Bioinformatics Center of Kyoto University, Japan. The significance threshold of enrichment analysis was set as p adjust *p* value ≤0.05 (Figures 3B,D).

GSEA is a calculation method used to determine whether a group of predefined genes shows a statistical difference between two biological states. It is usually used to estimate changes in pathways and biological process activities in expression dataset samples (Subramanian et al., 2005). To study the differences in biological processes between the two groups of patients, we used the gene expression profile dataset from the MSigDB database (Liberzon et al., 2015) (https://www.gsea-msigdb.org) (Figures 3E–G). The detailed information is shown in Supplementary Table S2.

2.1.4 NMF cluster analysis

Nonnegative matrix factorization, referred to as NMF, is a matrix factorization method proposed by Lee and Seung in the

journal Nature in 1999 (Lee and Seung, 1999). It makes all the decomposed components non-negative (requiring purely additive description), and at the same time realizes nonlinear dimension reduction. The samples were analyzed by NMF unsupervised cluster analysis, which was realized using the NMF package in R (v0.23.0) (Zushi, 2021). The correlation between the expression of PRR-DEGs and clinical features (including race, stage, age, and sex) based on NMF classification was visualized (Figures 4A–C). Gene set variation analysis, referred to as GSVA, is a non-parametric and unsupervised algorithm. Unlike GSEA, GSVA does not need to group samples in advance and can calculate the enrichment scores of specific gene sets in each sample. In other words, GSVA transforms gene expression data from a single gene as a feature expression matrix to a specific gene set as a feature expression matrix. To further analyze differences between NMF classifications, GSVA analysis was implemented using the GSVA package (v1.40.1). Finally, the features of NMF classification were visualized using the FactoMineR (v2.4) and factoextra packages (v1.0.7) (Figures 4D–F).

FIGURE 3
Enrichment results of GO, KEGG and GSEA. **(A)** GO enrichment analysis bar chart of up-regulated genes (TOP5 of BP, CC, and MF). **(B)** up-regulating the enrichment result of gene KEGG. **(C)** GO enrichment analysis bar chart of down-regulated genes (TOP5 of BP, CC and MF). **(D)** down-regulating the enrichment result of gene KEGG. **(E—G)**: GSEA analysis of TOP3 results.
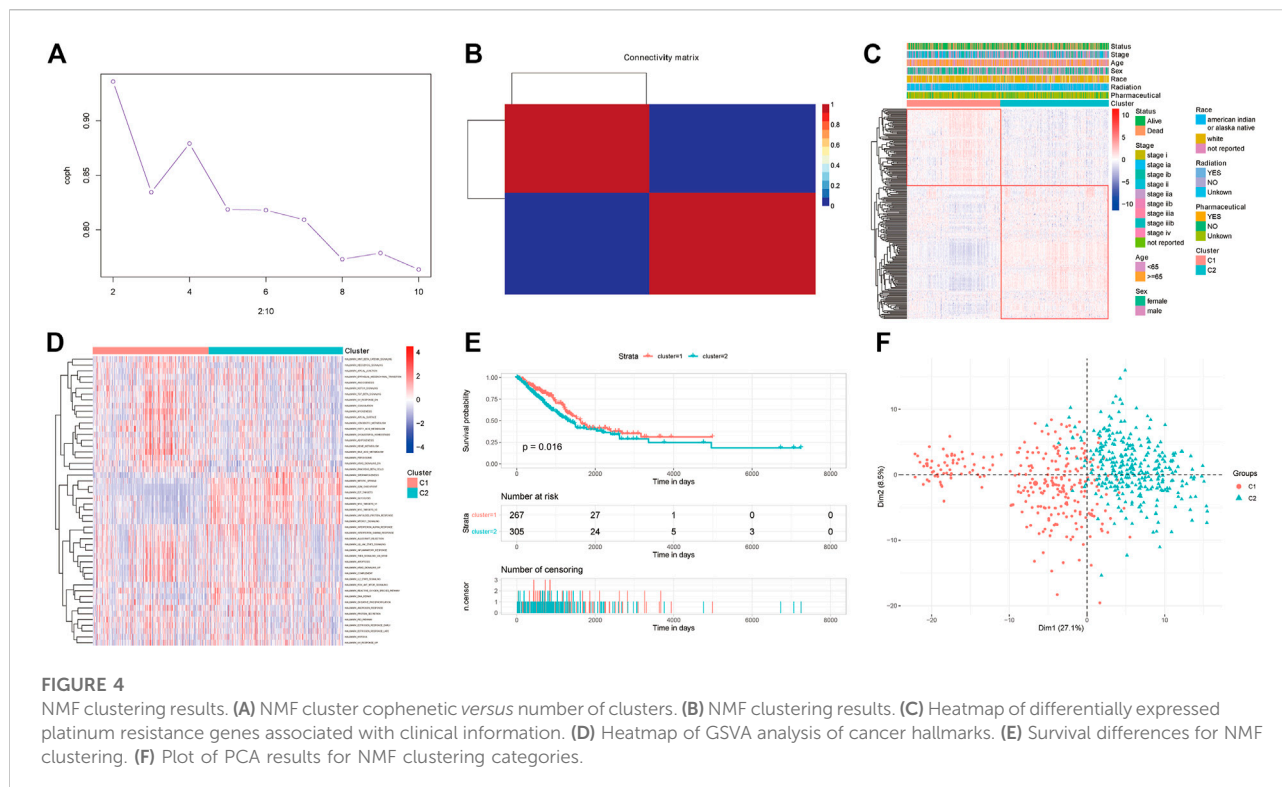
2.1.5 Prognostic model construction

Owing to the importance of platinum resistance in the treatment of LUAD, different patients may have different platinum resistance states; as such, it is extremely feasible to construct a diagnostic model based on differentially expressed platinum resistance genes. Here, firstly, we used the least absolute shrinkage and selection operator (LASSO) regression method to screen differentially expressed platinum resistance genes; the R package glmnet (v4.1–2) was used to realize this method and select the best lambda symbol value. After regression, only genes with coefficients other than 0 were retained (Figures 5A,B).

To analyze the relationship between the prognosis model and survival status, we used Kaplan–Meier survival analysis and risk factor analysis. Then, to verify the predictive efficiency of the diagnostic model, receiver operating characteristic (ROC) curves were drawn using the R package pROC (v1.18.0) (Robin et al., 2011). The area under the curve (AUC) of 1 year, 3 years, and 5 years were evaluated. To further prove the robustness of the model prediction, external data (GSE26939) were used for verification (Figures 5C–F).

To further verify the efficacy of the prognostic model of PRR-DEGs, we incorporated clinical indicators into the model, evaluated the univariate and multifactorial prognostic models of clinical factors using the survival package (v3.2.11), and displayed them as forest maps. In addition, we took clinical factors into account and used the rms package (v6.2-0) to construct clinical prediction nomogram and corresponding calibrate correction charts (Figures 5G,H).

We investigated whether clinical features are related to prognosis. Univariate Cox regression analysis showed that risk score, sample intermediate dimension, tumor stage, person

FIGURE 4
NMF clustering results. **(A)** NMF cluster cophenetic *versus* number of clusters. **(B)** NMF clustering results. **(C)** Heatmap of differentially expressed platinum resistance genes associated with clinical information. **(D)** Heatmap of GSVA analysis of cancer hallmarks. **(E)** Survival differences for NMF clustering. **(F)** Plot of PCA results for NMF clustering categories.

neoplasm cancer status were significantly correlated with OS (Figure 6A). Finally, these univariate prognostic variables were used as covariates of multiple cox regression analysis. The results showed that risk score and tumor status were independent prognostic factors related to OS (Figure 6B).

In order to evaluate whether our model can effectively predict the prognosis of patients in the clinical environment, we incorporated OS-related factors into the model and constructed a nomogram (Figure 6C) to predict the OS: 1, 3, and 5-year survival rates of patients. The nomogram model once again confirms the reliability and prospective clinical applicability of the risk model. At the same time, we Calibration the nomogram and found that the predicted results were highly correlated with the actual survival rate (Figure 6D).

2.1.6 Immune infiltration analysis

The immune microenvironment mainly consists of immune cells, inflammatory cells, fibroblasts, interstitial tissues, and various cytokines and chemokines, and is a loaded comprehensive system. The infiltration analysis of immune cells in tissues plays an important guiding role in disease research and treatment prognosis prediction.

To further explore the relationship between differentially expressed prognostic platinum resistance genes and the infiltration level of immune cells, CIBERSORT (Steen et al., 2020) was used to evaluate the infiltration level of immune cells. The contents of 22 kinds of immune cells in each patient were calculated based

on the LM22 background gene set provided by the CIBERSORT website (https://cibersort.stanford.edu/) to reflect the infiltration level. The results were visualized using box diagrams drawn by the R package ggplot2 (v3.3.5) (Figures 7A–D). Significant differences between high and low immune cell expression groups of patients may be related to the prognosis of PRR-DEGs. We used the R package ggExtra (v0.9) and a p-value < 0.01 to identify extremely significant differences in levels of immune cell infiltration, DEGs, and the prognosis of platinum resistance gene expression; the results were visualized using scatter plots and correlation curve fitting. At the same time, we checked the high- and low-risk groups of the immune checkpoints (CD274, CD47, HAVCR2, LAG3, IDO1, SIRPA, TNFRSF4, YTCN1, PDC D1, CTLA4, and TIGIT). The tumor immune dysfunction and exclusion (TIDE) score reflects the sensitivity to immune checkpoints, and the TIDE score calculated for each tumor sample could be used as a substitute biomarker to predict responses to immune checkpoint blocking (Figures 7E,F).

N-methyladenine (m6A) modification is the most common and abundant RNA modification in eukaryotes. To explore differences in m6A between high and low groups, we used m6A regulatory factor data from Yongsheng Li et al. (Li Y et al., 2019), including 11 readers, 7 writers, and 2 erasers.

2.1.7 Drug sensitivity analysis

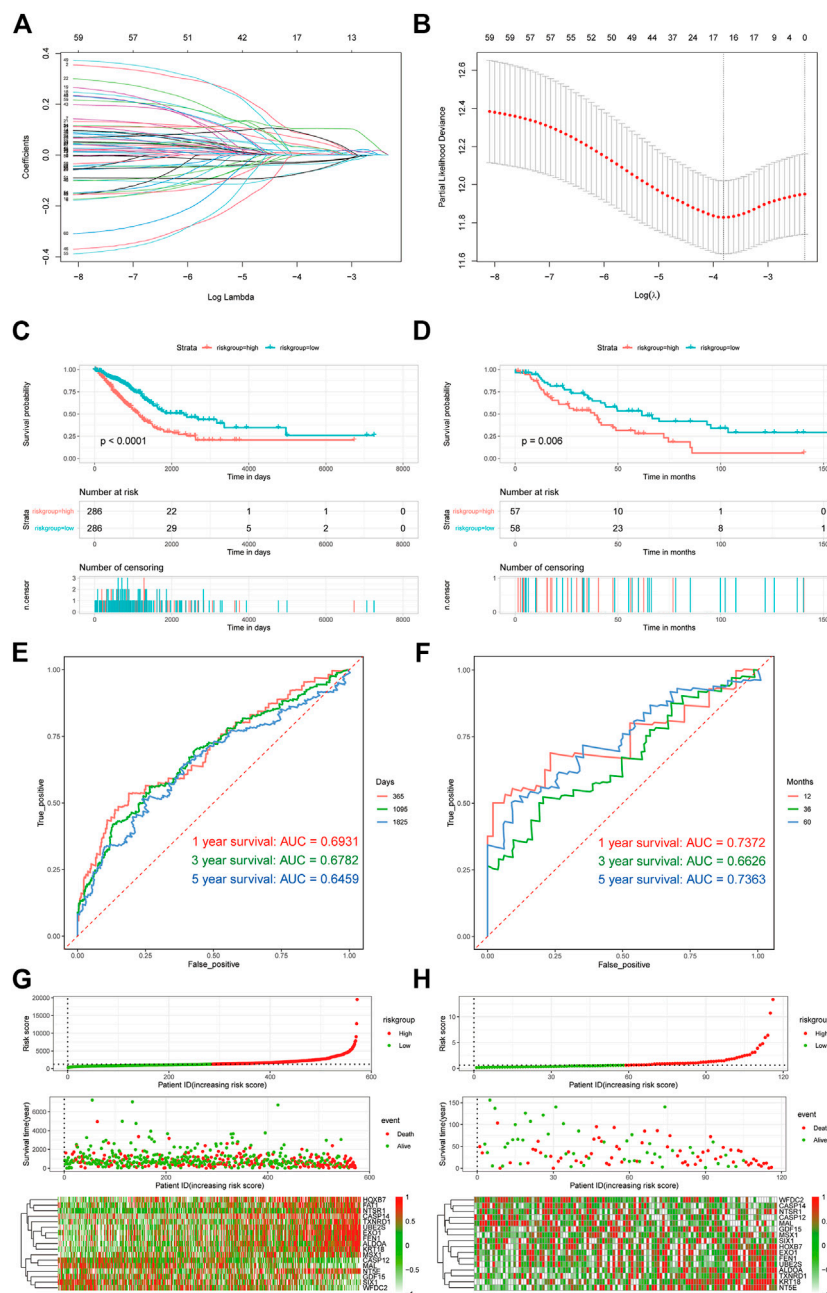The LUAD cell line-drug action dataset was obtained from the Genomics of Drug Sensitivity in Cancer database (GDSC

FIGURE 5
Construction and evaluation of prognostic models. **(A,B)** Lasso-cox regression analysis graph. **(C,D)** Survival analysis of TCGA LUAD and GSE16939. **(E,F)** Time ROC curve analysis of TCGA LUAD and GSE16939. **(G,H)** Association factor analysis of TCGA LUAD and GSE16939.

www.cancerRxgene.org) (Yang et al., 2012). The drug sensitivity of the expression data in TCGA-LUAD was analyzed using the R package oncoPredict (v0.2) (Maeser et al., 2021), and the sensitivity differences of high- and low-risk groups to different drugs were compared (Figure 9).

2.1.8 Construction of ceRNA network

To analyze the relationship between DEGs and miRNA and lncRNA in the post-transcriptional stage, we collected data from the Tarbase (https://dianalab.e-ce.uth.gr/html/diana/web/index.php?R=tarbasev8) (Karagkouni et al., 2018) and TargetScan (https://www.targetscan.org/vert_72/) (Agarwal et al., 2015) databases for miRNA
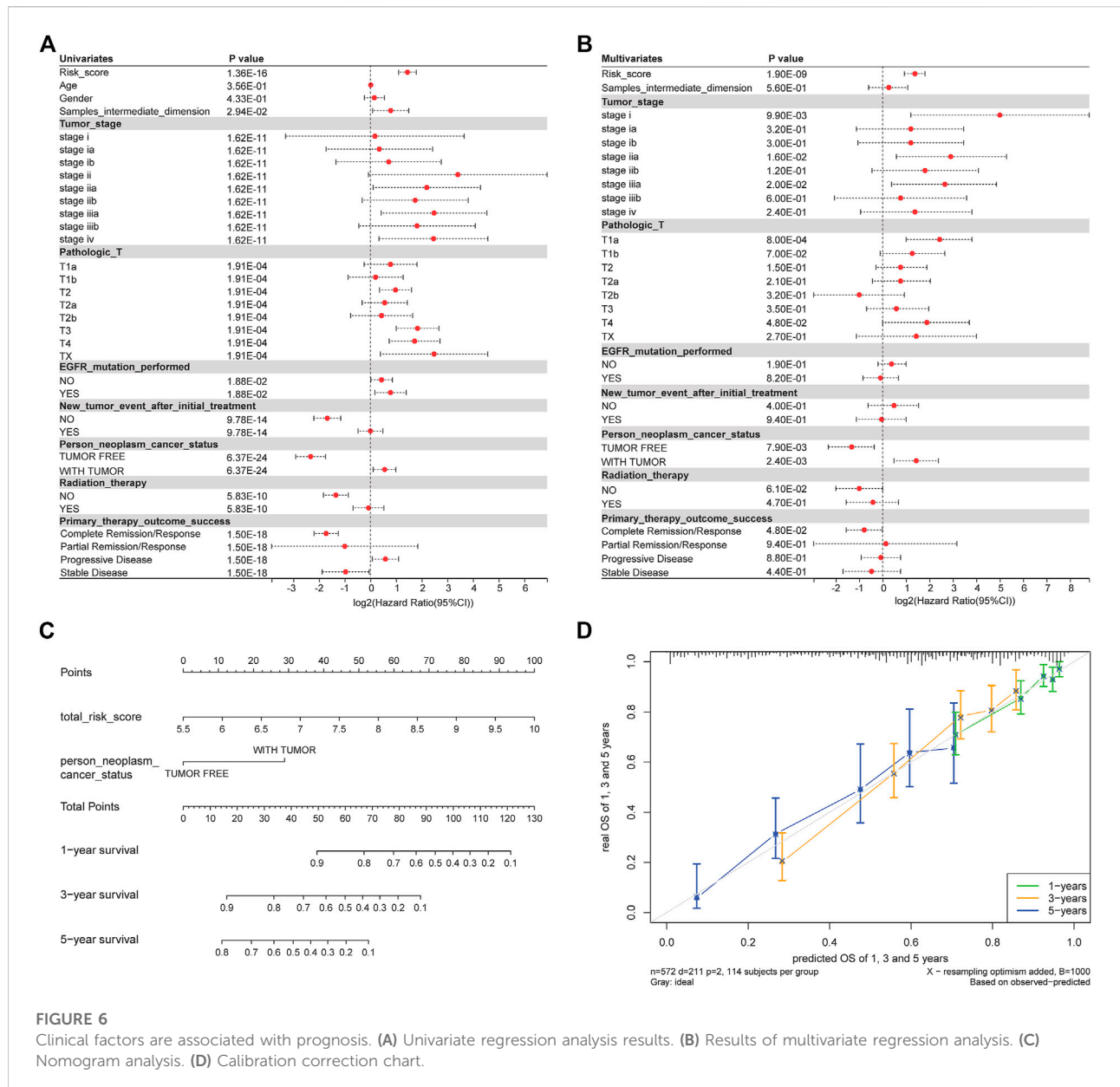
FIGURE 6
Clinical factors are associated with prognosis. **(A)** Univariate regression analysis results. **(B)** Results of multivariate regression analysis. **(C)** Nomogram analysis. **(D)** Calibration correction chart.

molecules that interact with PRR-DEGs. Using two databases improved the accuracy, and eulerr (v6.1.1) was used to draw the Wayne diagram. Then, using lncbase predicted v.2 (https://dianalab.e-ce.uth.gr/html/diana/web/index.php?R = lncbasev2/index-predicted) (Paraskevopoulou et al., 2016) and the StarBase V2.0 database (https://starbase.sysu.edu.cn/starbase2/index.php) (Maeser et al., 2021), we found that miRNA and lncRNA molecules can bind to, and then construct, the ceRNA network. In addition, we analyzed the expression differences of miRNA and lncRNA in the normal tumor group and divided the samples into high- and low-expression groups according to the average expression of miRNA and lncRNA. Finally, we performed Kaplan–Meier survival analysis (Figure 10).

2.1.9 Statistical analysis

All data calculations and statistical analyses are carried out in the R language (v4.1.0). For comparison between the two groups, we used a variance test, $p \leq 0.05$ was considered statistically significant.

3 Results

3.1 DEG analysis

To reveal biological differences between LUAD patients and healthy people at the transcriptome level, DEG analysis was conducted between the two groups. After screening by a
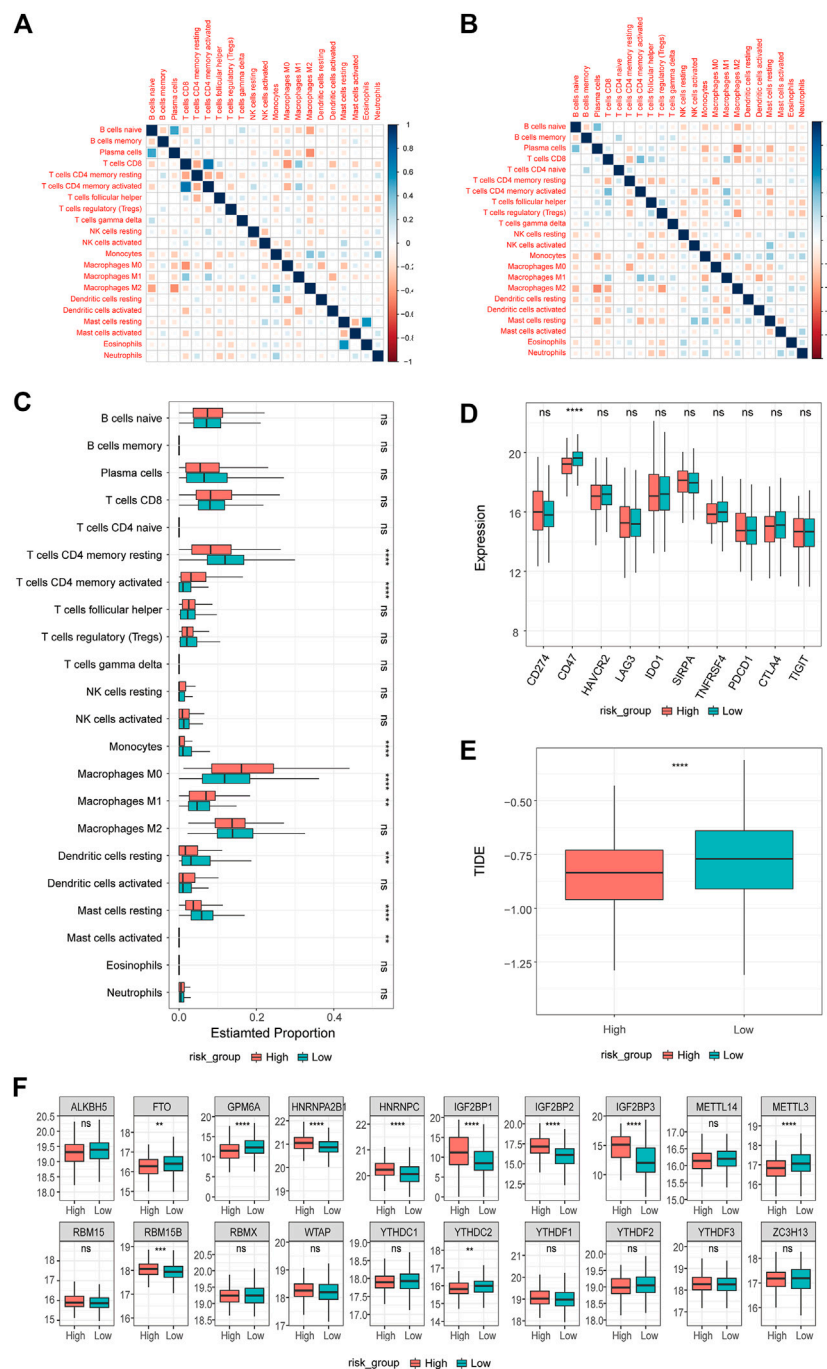
FIGURE 7
Results of immune infiltration analysis. **(A,B)** Correlation of immune infiltration in high-risk and low-risk groups. **(C)** Differences in immune infiltration between high and low risk groups. **(D)** Differences in immune checkpoints between high and low risk groups. Differences in **(E)** TIDE between high and low risk groups. Differences of **(F)** m6A regulon in high and low risk groups.

statistical significance threshold, a total of 252 genes were defined as platinum resistance genes with significant differential expression (Figures 2A,B), of which 161 were upregulated and 91 were downregulated. The PPI network diagram (Figure 2C) of PRR-

DEGs was constructed using the String database. In addition, we calculated the correlation of differentially expressed platinum resistance genes, and found that the correlation between upregulated and downregulated genes was closer (Figure 2D).

3.2 Functional enrichment analysis

In order to further reveal the biological functions and processes affected by the differential expression of platinum resistance genes, up-regulated and down-regulated genes were enriched by GO, KEGG, and GSEA and visualized in various forms. The enrichment results of up-regulated gene GO showed that TOP5 entries related to biological processes (BP) were double-strand break repair, DNA reconstruction, DNA replication, intrinsic apoptotic pathway, and a response to oxidative stress (Figure 3A), KEGG enriched to cell cycle, cellular senescence, IL-17 signaling pathway, p53 signaling pathway, platinum drug resistance *etc.* (Figure 3B). The down-regulated gene GO enriches the TOP5 items about biological processes (BP) as a response to lipopolysaccharide, muscle cell proliferation, response to molecule of bacterial origin, response to mechanical stimulus, and regulation of cell-cell adhesion (Figure 3C). Down-regulated gene KEGG enrichment is mainly related to the MAPK signaling pathway, IL-17 signaling pathway, EGFR tyrosine kinase inhibitor resistance, TNF signaling pathway, and other related pathways (Figure 3D). In addition, GSEA analysis showed that TOP3 was E2F targets, G2M checkpoint, TGFβ signaling pathway (Figures 3E–G).

3.3 NMF clustering analysis

We molecular-typed the data of TCGA-LUAD according to the PRR-DEGs. In the NMF method (Figure 4A), the abscissa corresponding to the first sharp decline of the cophenetic graph is the optimal cluster number. The results (Figure 4B) showed that the samples of LUAD could be divided into two categories. Then, we visualized the relationships between the PRR-DEGs and clinical information such as stage, race, age, and sex (Figure 4C), and identified that PRR-DEGs can basically be classified according to NMF. In addition, we calculated the GSVA analysis scores of cancer hallmarks (Figure 4D). WNT beta-catenin signaling and hedgegcg signaling, among others, scored higher in the C1 category, g2 checkpoint and e2f targets, among others, scored higher in the C2 category. The survival analysis of the two classifications of NMF (Figure 4E) showed that the survival rate of C1 was slightly higher than that of C2, and was statistically significant (*p* < 0.05). Principal component analysis (PCA) analysis suggested that most samples of the two categories of NMF can be separated (Figure 4F).

3.4 Construction and evaluation of prognosis model

We constructed a prognosis model based on the PRR-DEGs in order to translate the research results into practical clinical application. First, 252 PRR-DEGs were screened using the LASSO regression method (Figures 5A,B). There were 17 genes with non-zero retention coefficients; therefore, we constructed a prognosis model with 17 genes, and the influence coefficient of each gene was the coefficient of the LASSO regression results. To verify the prognostic efficacy of the prognostic model, survival analysis (Figures 5C,D) was carried out based on TCGA-LUAD data and the validation dataset (GSE26939). The survival of the high-risk group was poor. In addition, the predicted ROC curve was drawn and the AUC was calculated. The results show that the prediction model has excellent prediction efficiency for both sets of data, and the AUC was ~0.7 (Figures 5D–F). Finally, in order to evaluate the correlation trend between each gene and risk score, risk factor analysis (Figures 5G,H) was carried out. Genes such as HOXB7, NT5E, and KRT18 were positively correlated with risk score in the two groups of data.

We investigated whether clinical features are related to prognosis. Univariate Cox regression analysis showed that the prognosis model gene, KRAS mutation, stage, and so on, were significantly correlated with OS (Figure 6A). Finally, these univariate prognostic variables were used as covariates of multivariate Cox regression analysis. The results showed that all of the prognostic model genes except CASP14 were independent prognostic factors related to OS (Figure 6B). The 17 genes are ALDOA, CASP12, CASP14, EXO1, FAT1, FEN1, GDF15, HOXB7, KRT18, MAL, MSX1, NT5E, NTSR1, SIX1, TXNRD1, UBE2S, and WFDC2. The risk score formula is risk score = 0.118495*exp (ALDOA) - 0.003607*exp (CASP12) + 0.01103671*exp (CASP14) - 0.03671*exp (EXO1) + 0.074027*exp (FAT1) + 0.058166*exp (FEN1) - 0.04225*exp (GDF15) + 0.061475*exp (HOXB7) + 0.105,367*exp (KRT18) - 0.10004*exp (MAL) + 0.134,121*exp (MSX1) + 0.099919*exp (NT5E) + 0.014771*exp (NTSR1) - 0.11253*exp (SIX1) + 0.024867*exp (TXNRD1) + 0.042712*exp (UBE2S) - 0.04043*exp (WFDC2).

To evaluate whether our model could effectively predict the prognosis of patients in clinical environments, we incorporated OS-related factors into the model and constructed a Nomogram (Figure 6C) to predict OS 1-, 3-, and 5-year survival rates. The Nomogram model again confirmed the reliability and prospective clinical applicability of the risk model. At the same time, upon calibration to the Nomogram, the predicted results were highly correlated with the actual survival rate (Figure 6D).

3.5 Immune infiltration analysis

To further explore the degree of immune cell infiltration in patients, the CIBERSORT method was used to calculate the degree of infiltration in all samples based on 22 kinds of background genes of immune cells. First, the correlation between the infiltration degree of immune cells in high- and

low-risk groups (Figures 7A,B) was calculated. In the high- or low-risk group, the correlation between macrophage M, naïve B cells, and plasma cells was high. In addition, we examined the differences in immune cell infiltration for the different groups (Figure 7C) and found significant differences in 8 of the 22 kinds of immune cells in both groups. Resting T cells CD4 memory, resting dendritic cells, resting mast cell, and monocytes have a higher degree of infiltration in the low-risk group, while T cells CD4 memory activated, macrophage M0, macrophage M1, and mast cell activated have a higher degree of infiltration in the high-risk group. In addition, we examined the differential expression of ten common immune checkpoints in the high- and low-risk groups (Figure 7D) and found that only CD47 was highly expressed in low-risk groups. We further explored the differences in TIDE scores between the two groups (Figure 7E) and found that the TIDE score of the low-risk group was higher. Then, we analyzed the differences in m6A regulatory factors between the high- and low-risk groups (Figure 7F)and found that FTO, GPM6A, METTL3, and YTHDC2 were higher in the low-risk group, while HNRNPA2B1, HNRNPC, TGF2BP1, IGF2BP2, IGF2BP3, and RBM15B were higher in the high-risk group.

Finally, to reveal the relationship between the expression of 17 prognostic platinum resistance genes and the infiltration level of immune cells more directly, a scatter plot was drawn and the correlation curve was fitted by taking the expression values of 8 significant differential immune cells and prognostic platinum resistance genes in the CIBERSORT results. The results showed that the average expression value of prognostic platinum resistance genes was positively correlated with macrophage M0, macrophage M1 and T cells CD4 memory activated (Figures 8A–C), while mast cell resting, monocytes and T cells CD4 memory resting were negatively correlated (Figures 8D–F). Then, to further identify drugs that may interact with the high-risk group, we identified the drug sensitivity of TCGA-LUAD patients (Figure 9) according to the gene expression data of TCGA-LUAD patients and the GDSC database. The results showed that the high-risk group was sensitive to drugs ABT7371910, Axitinib1021, Afatinib1032, Afuresertib1912, Axitinib1021, Ipatasertib1924, and Ibrutinib1799, and had lower IC50 (Figure 9A). In contrast, the high-risk group was nonsensitive to Afatinib1032, Bortezomib1191, Dasatinib1079, Docetaxel1007, Erlotinib1168, Gefitinib1010, Lapatinib1558, ZM4474391050, Paclitaxel1080, and Tozasertib1096 (Figure 9B).

3.6 ceRNA network construction

In total, 17 PRR-DEGs related to prognosis were identified, 5 mi-RNA (Figure 10A) interacting with PRR-DEGs were identified based on Tarbase and Targetscan databases, and 18 lncRNA (Figure 10D) interacting with miRNA were found through lncBase predicted V.2 and the StarBase V2.0 databases,

which constituted the ceRNA network. The difference in expression of lncRNA and miRNA between the acute tumor group and normal group (Figure 10B, C), as well as the KM survival of high- and low-risk groups, were analyzed. The results showed that among the five mi-RNA, only has-miR-374a-5p had different expression and survival curves between the tumor group and the normal group. The expression of HAS-MIR-374a-5P in the tumor group was lower, but its survival in the high-expression group was worse (Figure 10E). The expression of RP6-24A23.7 in lncRNA was also lower in the tumor group, and the prognosis was worse in the high expression group (Figure 10F).

4 Discussion

Although the incidence of lung cancer is lower than that of female breast cancer, the mortality rate remains the highest worldwide (Xia et al., 2022). In China, the lung cancer death rate is the highest among all cancers (Miller et al., 2016). Until 1995, landmark meta-analysis confirmed that cisplatin-based chemotherapy could significantly prolong the survival of NSCLC patients compared with meta-supportive treatment (Listed, 1995). Subsequent studies further confirmed the importance of chemotherapy in the treatment of NSCLC (Socinski et al., 2013). Since then, targeted therapies and immunotherapies have been developed. However, many patients cannot use targeted drugs because they are resistant to the drugs or because they contain driving genes; moreover, immunotherapy cannot be used because of unqualified immune indexes. As such, chemotherapy remains the best option for these patients, despite its toxic nature and strong side effects. Cisplatin-based chemotherapy is still the main method for the treatment of many cancers, but patients treated with platinum drugs will inevitably develop drug resistance.

In this study, we explored the mechanisms of drug resistance, prolonged drug resistance time, and longer survival time for patients. M6A is a methylation modification of RNA adenine (A), which is one of the most abundant modifications in eukaryotic mRNA. It is mainly regulated by the m6A methylation regulator (Chen et al., 2019; Liu et al., 2019). Previous studies have focused on the relationship between m6A and the occurrence and development of LUAD (Li et al., 2022; Ma et al., 2022; Qian et al., 2021), or the relationship between the m6A regulatory factor and chemotherapy resistance of small cell lung cancer (Zhang et al., 2021a; Zhang et al., 2021b). Some studies have also found that the m6A regulatory factor is closely related to LUAD resistance to erlotinib (Li K et al., 2021). As far as we know, our study is the first to explore the relationship between m6A and LUAD resistance to platinum. Some past studies have found that FTO promotes the growth of lung cancer cells (Li J et al., 2019), but in this study, the expression of FTO in the low-risk group was higher than that in the high-risk group, which suggests that the
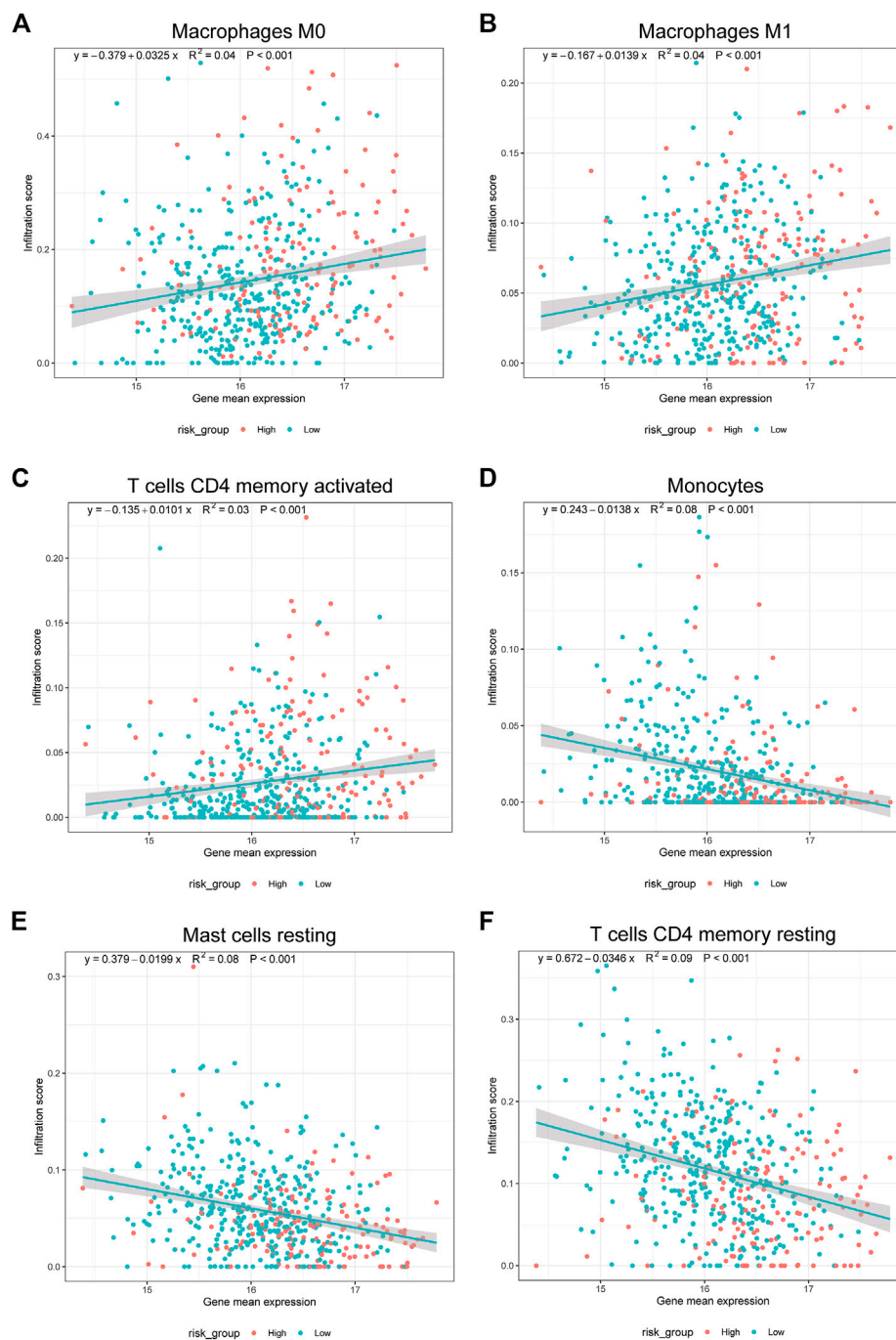
FIGURE 8
Prognostic model genes associated with immune cells. **(A–F)**. Correlation of mean gene expression in prognostic model with Macrophage M0, Macrophage M1, mast cell resting, Monocytes, T cells CD4 memory activated, T cells CD4 memory resting.

m6A regulatory gene may have changed in platinum-resistant patients with LUAD.

In this study, by comparing the genes of LUAD patients from the TCGA database with platinum resistance genes from A database of genes related to platinum resistance, 252 platinum resistance genes with significant differential expression were obtained, of which 161 were upregulated and 91 were downregulated. Among the significantly different drug resistance genes, LIN28B is the most upregulated gene. LIN28, a structurally conserved RNA-binding protein, is highly
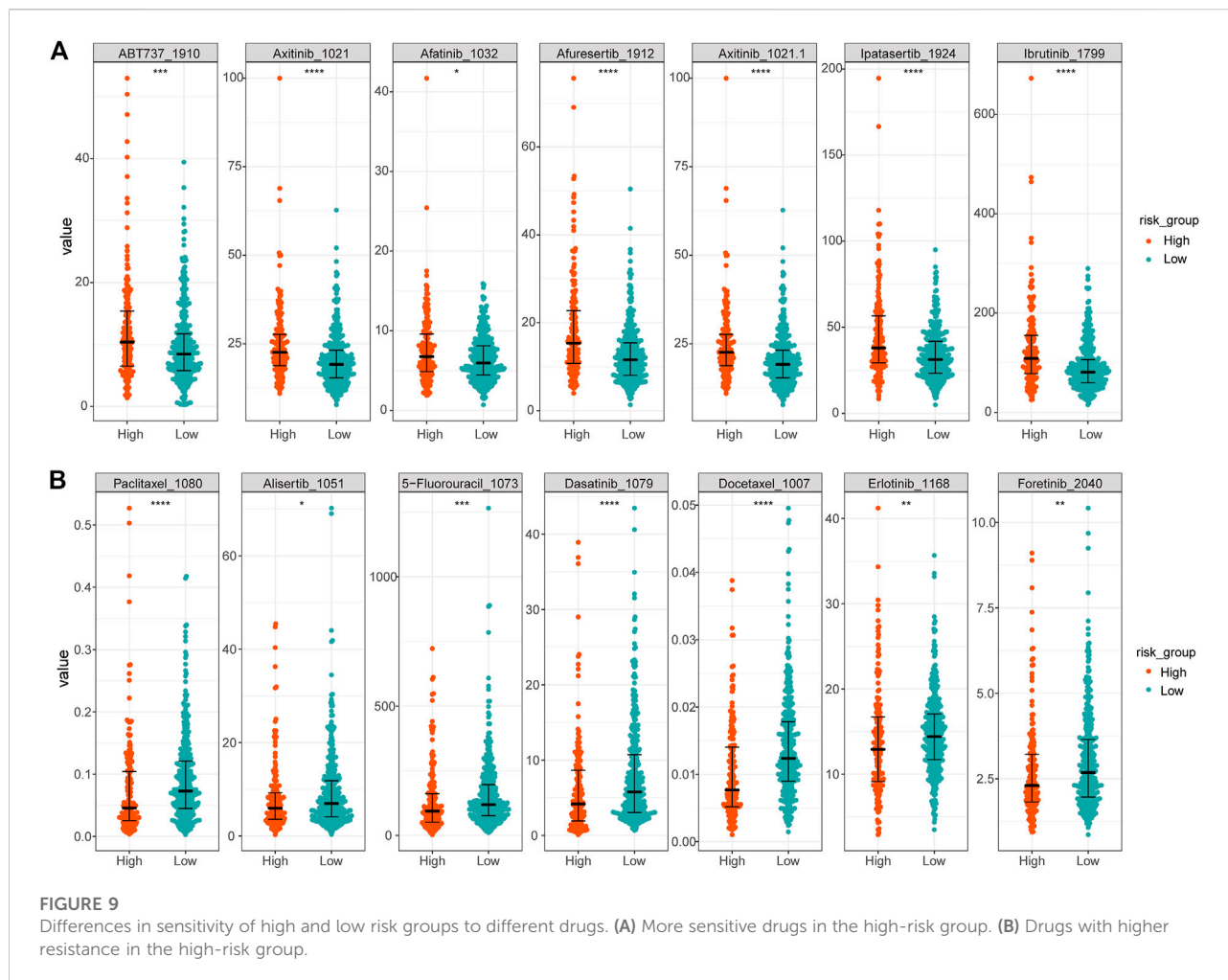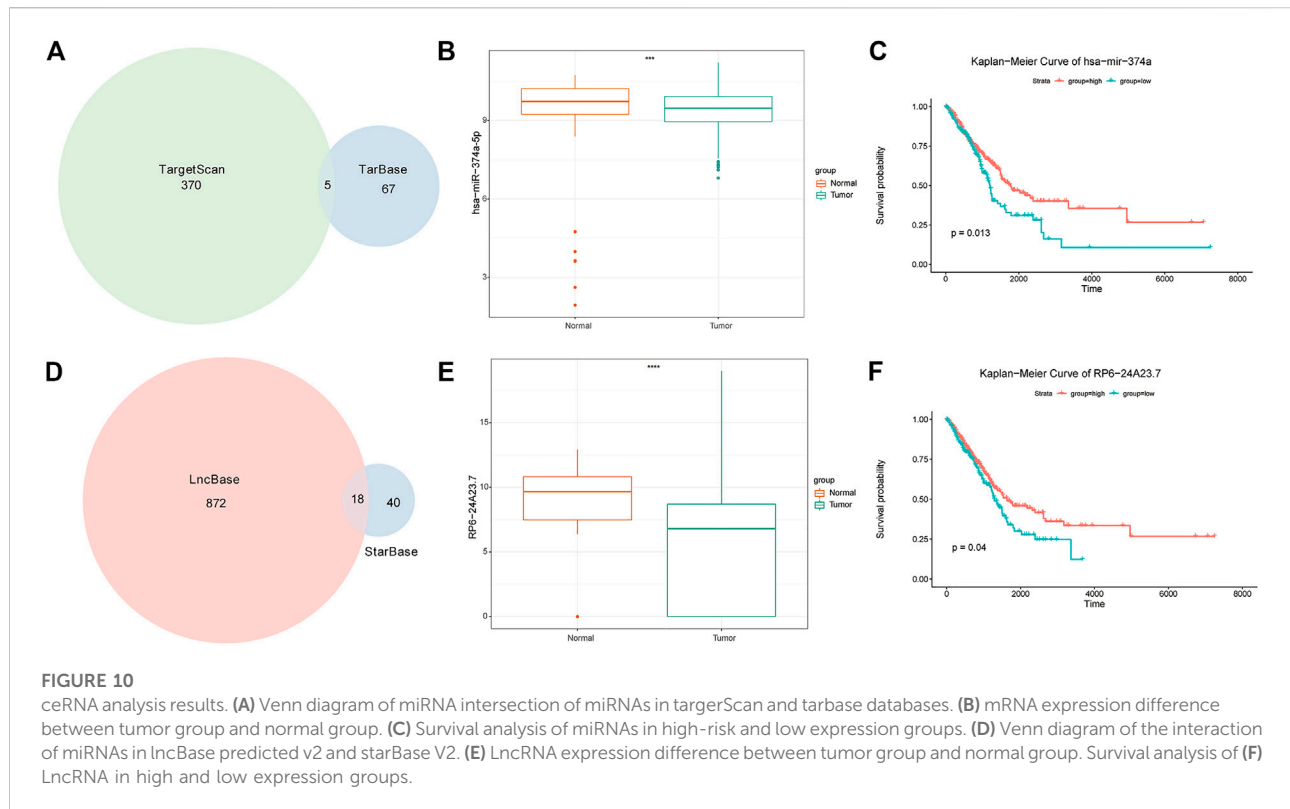
FIGURE 9
Differences in sensitivity of high and low risk groups to different drugs. **(A)** More sensitive drugs in the high-risk group. **(B)** Drugs with higher resistance in the high-risk group.

expressed in embryonic hepatocytes. It can promote rapid cell proliferation and is highly expressed in a variety of tumor tissues and tumor cell lines. The high expression of the LIN28 gene can increase the ability of liver cancer cells to metastasize to distant places (McDaniel et al., 2016), moreover, LIN28 can increase the resistance of ovarian and breast cancer cells to chemotherapy drugs by regulating let-7i (Yang et al., 2008). High expression of LIN28 can increase the insensitivity of lung cancer cells and pancreatic cancer cells to radiotherapy (Oh et al., 2010). However, when LIN28 is inhibited, the growth of NSCLC is reduced (Yang et al., 2019). Our research indicates that the high expression of LIN28B may lead to an increase in the resistance of LUAD cells to platinum drugs. This is helpful for further verification in subsequent experiments.

A PPI network diagram of upregulated and downregulated genes was constructed, and correlation analysis showed that the correlation between upregulated and downregulated genes was greater. The essence of oxidative stress is the imbalance of the oxidation–antioxidation system *in vivo*. However, the intracellular oxidation–reduction system of many tumor cells

is out of balance, and so the drug resistance of LUAD cells is also closely related to oxidative stress (Winterbourn, 2008). There is DNA recombination in the GO pathway of gene enrichment, and the study shows that the occurrence and development of lung adenocarcinoma are closely related to it (Liang et al., 2022). We speculate that platinum resistance of lung adenocarcinoma is also closely related to it, and we will focus on it in the follow-up research. The research and development of lipopolysaccharide drugs have further improved drug utilization (Guo et al., 2019). In our down-regulated gene GO enrichment, top1 is the reaction pathway to lipopolysaccharide. We speculate that in patients with lung adenocarcinoma drug resistance, the metabolism of lipopolysaccharide substances decreases, which may lead to resistance to platinum drugs, which has a certain hint for us to improve platinum drugs. The top three GSEA enrichment sites were e2f targets, g2m checkpoint, and rgf beta signaling. E2f is a transcription factor gene family. Previous research found that E2F can regulate the expression of mitochondria-related genes, and the loss of this regulation leads to serious mitochondrial defects that affect cell metabolism and tumor cells

FIGURE 10
ceRNA analysis results. **(A)** Venn diagram of miRNA intersection of miRNAs in targerScan and tarbase databases. **(B)** mRNA expression difference between tumor group and normal group. **(C)** Survival analysis of miRNAs in high-risk and low expression groups. **(D)** Venn diagram of the interaction of miRNAs in lncBase predicted v2 and starBase V2. **(E)** LncRNA expression difference between tumor group and normal group. Survival analysis of **(F)** LncRNA in high and low expression groups.

(Benevolenskaya and Frolov, 2015). Yao et al. (Yao et al., 2020) found that E2F, the most abundant pathway in our GSEA analysis, is a potential biomarker and therapeutic target of colon cancer, which indicates that LUAD resistance to platinum is also closely related to the E2f family. The G2m checkpoint pathway is an important part of the cell cycle and is related to the occurrence and development of many tumors. A High G2M score is always related to the overall survival rate of pancreatic cancer (Oshi et al., 2020).

NMF, which can be used to solve the complex and excessive calculation issues caused by huge data, is a decomposition non-probability algorithm using matrix decomposition, belonging to the linear algebra algorithm group (Egger, 2022). NMF processes the data after TFIDF conversion by decomposing a matrix into two low-level matrices (Obadimu, 2019). We used the NMF algorithm for the molecular typing of PRR-DEGs and found that LUAD samples could be divided into two categories. We then used heatmap visualization to identify associations between PRR-DEGs and clinical information such as stage, race, age, and sex. Using PCA, we also found that the two categories of samples could be distinguished easily. In GSVA analysis, 4dk wnt beta-catenin signaling and hedgegcg signaling had the highest scores in C1. Wnt/β-catenin is a classic signal pathway, and the occurrence and development of many tumors are closely related to it, including colon cancer, hepatocellular carcinoma, desmoid tumor, pancreatic cancer, gastric cancer, melanoma,

ovarian cancer, renal cancer (Guillen-Ahlers,2008), and prostate cancer (Robinson et al., 2008). Our analysis shows that the platinum resistance of LUAD is also related to Wnt/β. In contrast, g2 eckpoint and e2f scored higher in C2. Some studies (Li S et al., 2021) have shown that the expression of abnormal cyclin G2 is the key factor leading to the pathological process of cancer, including glioma. Among the platinum resistance genes in LUAD, the related gene of cyclin G2 is also very important and warrants attention.

To better guide clinical work, we constructed a prognostic model to evaluate the PRR-DEGs, and screened 252 PRR-DEGs using the LASSO regression method. There were 17 genes with a non-zero retention coefficient, and so we constructed a prognostic model with 17 genes; the influence coefficient of each gene was the coefficient of the LASSO regression results. Based on TCGA-LUAD data and a validation set (GSE26939), survival analysis was carried out to verify the prognostic efficacy of the prediction model, which confirmed that the prognosis of the high-risk group was poor. Moreover, risk factor analysis was used to evaluate the correlation trend between each gene and risk score. We found that genes such as HOXB7, NT5E, and KRT18 were positively correlated with risk score. Studies (Yan et al., 2022) have shown that the HOXB gene cluster contributes to cancer development; increased expression of HOXB3, HOXB6, HOXB7, HOXB8, and HOXB9 in LUAD patients is linked with poor overall survival (OS). Our data mining also illustrated the close relationship between the

HOXB7 gene and LUAD platinum resistance. Past research (Dong et al., 2020) has also shown that NT5E levels are significantly higher in NSCLC tissues and cells. In our model, NT5E was also associated with the platinum resistance of LUAD, suggesting that the NT5E gene may be related to the development of lung cancer. The study has shown that the overexpression of ALDOA increases the migration and invasion of lung cancer cell lines *in vitro* and the formation of metastatic lung cancer *in vivo* (Chang et al., 2019). Our analysis suggests that ALDOA may also be associated with platinum drug resistance. Cystatin (CASPs) is an important regulator and executor of the apoptosis pathway. It has been found that the CASP family is closely related to the prognosis of non-small cell lung cancer (Lee et al., 2010). However, there is no study to explore the relationship between CASP and platinum resistance. Our analysis shows that CASP12, and CASP14 may be related to platinum resistance. This will guide the following research. The researchers have found that the deletion of FAT1 can accelerate the occurrence and malignant progression of tumors. In mouse and human squamous cell carcinomas, the loss of FAT1 function can promote tumorigenesis by inducing a mixed EMT state (Pastushenko et al., 2021). The other study has shown that FAT1 mutation is associated with better immunogenicity and ICI efficacy, which may be considered as a biomarker of patients who choose to receive immunotherapy (Zhang et al., 2022). The results of the expression of the same gene will be different under different treatment regimens. No one has studied the relationship between FAT1 and platinum resistance.FEN1 is the main component of the basic excision and repair pathway of the DNA repair system. Studies have shown that the high expression of the FEN1 gene is essential for the rapid proliferation of lung cancer cells, and the FEN1 gene can also increase the resistance of lung cancer cells to cisplatin (He et al., 2017). Studies have shown that the over-expression of GDF15 significantly inhibits the proliferation of NSCLC *in vitro* and *in vivo* (Lu et al., 2018). Through our analysis and prediction, GDF15 may be also related to platinum resistance of lung adenocarcinoma, which needs further verification by subsequent experiments. Studies have shown that high TXNRD1 protein levels are associated with shorter disease-free survival and postoperative distal metastasis-free survival in patients with NSCLC, including some individuals receiving platinum adjuvant chemotherapy (Delgobo et al., 2021; Guo et al., 2021), indicating that TXNRD1 is an important predictor of poor prognosis, which is consistent with our conclusion. Some studies have shown that UBE2S promotes the metastasis of lung adenocarcinoma cells by activating NF- κ B signal transduction, while other studies have shown that UBE2S regulates Wnt/β-catenin signal and promotes the progression of non-small cell lung cancer (Ho et al., 2021; Qin et al., 2020).In our predictive model, UBE2S is also an important factor in platinum resistance in patients with lung adenocarcinoma. The clinical prediction model established by Luo Yu et al. also shows that WFDC2 is an important factor affecting the prognosis of lung adenocarcinoma. Whether WFDC2 is also an important factor affecting platinum resistance in lung adenocarcinoma needs

further experimental verification (Luo et al., 2022). Univariate Cox regression analysis showed that prognostic model genes, KRAS mutations, stages, and so on, were significantly correlated with OS. These univariate prognostic variables were used as covariates of multivariate Cox regression analysis. Except for CASP14, the other 16 prognostic model genes were independent prognostic factors related to OS. The nomogram model once again confirmed the reliability and prospective clinical applicability of the risk model. When the nomogram was used for calibration, the predicted results were highly correlated with the actual survival rate. This shows that our risk model has good clinical application value.

Focusing on the immune status of tumor patients will help us to explore the mechanisms of drug resistance and new therapeutic targets. Therefore, we used the CIBERSORT method to calculate the infiltration degree of immune cells in all samples; the results showed that resting T cells CD4 memory, resting dense cells, resting mast cell, and monocytes had higher infiltration degrees in the low-risk group than in the high-risk group. While activated T cells CD4 memory, macrophage M0, macrophage M1, and activated mast cells had higher infiltration degrees in the high-risk group compared with the low-risk group. From a scatterplot of the above eight different immune cells and platinum resistance genes, the average expression values of platinum resistance genes in prognosis were positively correlated with macrophage M0, macrophage M1 and activated T cells CD4 memory but negatively correlated with resting mast cell, monocytes, and resting T cells CD4 memory.

The TIDE score can be used to evaluate the potential clinical efficacy of immunotherapy in different immune-related gene prognostic model (IRGPI) subsets (Liu, 2018). The higher the TIDE prediction score, the higher the possibility of immune escape, suggesting that patients are less likely to benefit from immunotherapy. Compared with the high-risk group, the low-risk group had higher TIDE scores, indicating that people in the low-risk group were more likely to experience immune escape and could not benefit from immunotherapy. N6-methyladenosine, also called m6A, is a base modification widely existing in mRNA. The internal modification of mRNA can affect the RNA splicing, translation, stability, and epigenetics of some non-coding RNAs (Meyer and Jaffrey, 2017). By analyzing the differences in m6A regulatory factors between high- and low-risk groups, it was found that FTO, GPm6A, METTL3, and YTHDC2 expression was higher in the low-risk group. Among these, studies have shown that FTO plays the role of an oncogene in acute myeloid leukemia (Li et al., 2017) by regulating the level of m6A and promoting the occurrence and development of leukemia. Later, other studies showed that FTO plays a role as m6A demethylase in various life processes (Gokhale et al., 2016; Xiang et al., 2017). However, in this study, FTO was highly expressed in the low-risk group. We suggest that FTO is not closely related to platinum drug resistance in LUAD. The expressions of HNRNPA2B1, HNRNPC, TGF2BP1, IGF2BP2, IGF2BP3, and RBM15B were higher in the high-risk group, indicating that the above m6A regulatory factors play an

important role in the mechanism of platinum resistance in LUAD. From drug sensitivity analysis, the high-risk group had lower IC50 to the drugs ABT7371910, Axitinib1021, Afatinib1032, Afuresertib1912, Axitinib1021, Ipatasertib1924, and Ibrutinib1799, indicating that the high-risk group is more sensitive to these drugs, but less sensitive to Afatinib1032, Bortezomib1191, Dasatinib1079, Docetaxel1007, Erlotinib1168, Gefitinib1010, Lapatinib1558, ZM4474391050, Paclitaxel1080, and Tozasertib1096. This has a certain clinical guiding significance for patients with LUAD after platinum resistance. Has-miR-374a-5p is related to the occurrence and development of pancreatitis (Wen et al., 2019), but the relationship between has-miR-374a-5p and platinum drug resistance of LUAD has not been explored. ceRNA analysis showed that has-miR-374a-5p is highly expressed in healthy individuals, and the higher the expression, the better the survival. RP6-24A23.7 is associated with lymphatic metastasis of LUAD (Yan et al., 2017). Morever, as we have demonstrated, may also be associated with platinum resistance in LUAD. The expression of RP6-24A23.7 was lower in the tumor group, and the survival was worse in the low expression group. These indicate that has-miR-374a-5p and RP6-24A23.7 were protective factors.

However, our research also had some limitations. First, in order to fully clarify the molecular mechanisms of resistance and development of platinum drugs in LUAD, microarray samples from platinum drugs in different degrees of LUAD are needed. Second, many biomarkers related to platinum resistance in LUAD still have no characteristics, and further bioinformatic analyses and experimental verifications are needed to clarify the biological function of these predictive genes in platinum resistance in LUAD. Unfortunately, because of the COVID-19 epidemic, our basic experimental process has been hindered. In future research, we will further use experiments to verify the mechanisms of drug resistance.

In summary, this study explored the characteristics of high- and low-risk groups by analyzing the biological process characteristics of platinum resistance genes in LUAD, established a prognosis model, and analyzed its m6A regulatory factors, immune infiltration, and drug sensitivity. Our results have significance for guiding clinical practice. We identified the potential targets and mechanisms of LUAD platinum resistance, laying the foundation for further research.

Data availability statement

Publicly available datasets were analyzed in this study. This data can be found here: TCGA (https://tcga-data.nci.nih.gov/tcga/), A database of genes related to platinum resistance (http://ptrc-ddr.cptac-data-view.org), GEO (https://www.ncbi.nlm.nih.gov/geo/query/acc.cgi?acc=GSE26939).

Ethics statement

Author contributions

Funding

Conflict of interest

The authors declare that the research was conducted in the absence of any commercial or financial relationships that could be construed as a potential conflict of interest.

Publisher's note

All claims expressed in this article are solely those of the authors and do not necessarily represent those of their affiliated organizations, or those of the publisher, the editors and the reviewers. Any product that may be evaluated in this article, or claim that may be made by its manufacturer, is not guaranteed or endorsed by the publisher.

Supplementary material

The Supplementary Material for this article can be found online at: https://www.frontiersin.org/articles/10.3389/fgene.2022.993322/full#supplementary-material

References

Agarwal, V., Bell, G. W., Nam, J., and Bartel, D. P. (2015). Predicting effective microRNA target sites in mammalian mRNAs. *eLife* 4. doi:10.7554/eLife.05005

Benevolenskaya, E. V., and Frolov, M. V. (2015). Emerging links between E2F control and mitochondrial function. *Cancer Res.* 75 (4), 619–623. doi:10.1158/0008-5472.CAN-14-2173

Chang, Y., Chiou, J., Yang, Y., Su, C., Lin, Y., Yang, C., et al. (2019). Therapeutic targeting of aldolase a interactions inhibits lung cancer metastasis and prolongs survival. *Cancer Res.* 79 (18), 4754–4766. doi:10.1158/0008-5472.CAN-18-4080

Chen, X., Zhang, J., and Zhu, J. (2019). The role of m6A RNA methylation in human cancer. *Mol. Cancer* 18 (1), 103. doi:10.1186/s12943-019-1033-z

Cui, Q., Shi, H., Ye, P., Li, L., Qu, Q., Sun, G., et al. (2017). M 6 a RNA methylation regulates the self-renewal and tumorigenesis of glioblastoma stem cells. *Cell Rep.* 18 (11), 2622–2634. doi:10.1016/j.celrep.2017.02.059

Delgobo, M., Gonçalves, R. M., Delazeri, M. A., Falchetti, M., Zandoná, A., Nascimento Das Neves, R., et al. (2021). Thioredoxin reductase-1 levels are associated with NRF2 pathway activation and tumor recurrence in non-small cell lung cancer. *Free Radic. Biol. Med.* 177, 58–71. doi:10.1016/j.freeradbiomed.2021.10.020

Dong, L., Zheng, J., Gao, Y., Zhou, X., Song, W., and Huang, J. (2020). The circular RNA NT5E promotes non-small cell lung cancer cell growth via sponging microRNA-134. *Aging* 12 (4), 3936–3949. doi:10.18632/aging.102861

Du, J., Hou, K., Mi, S., Ji, H., Ma, S., Ba, Y., et al. (2020). Malignant evaluation and clinical prognostic values of m6A RNA methylation regulators in glioblastoma. *Front. Oncol.* 10, 208. doi:10.3389/fonc.2020.00208

Egger, R. (2022). "Modelling hidden semantic structures in textual data," in *Applied data science in tourism* (Switzerland: Springer Nature). doi:10.1007/978-3-030-88389-8_18

Geng, Y., Guan, R., Hong, W., Huang, B., Liu, P., Guo, X., et al. (2020). Identification of m6A-related genes and m6A RNA methylation regulators in pancreatic cancer and their association with survival. *Ann. Transl. Med.* 8 (6), 387. doi:10.21037/atm.2020.03.98

Gokhale, N. S., McIntyre, A. B. R., McFadden, M. J., Roder, A. E., Kennedy, E. M., Gandara, J. A., et al. (2016). N6 -Methyladenosine in flaviviridae viral RNA genomes regulates infection. *Cell Host Microbe* 20 (5), 654–665. doi:10.1016/j.chom.2016.09.015

Guillen-Ahlers, H. (2008). Wnt signaling in renal cancer. *Curr. Drug Targets* 9 (7), 591–600. doi:10.2174/138945008784911813

Guo, L., Zhang, Y., Wei, R., Wang, C., and Feng, M. (2019). Lipopolysaccharide-anchored macrophages hijack tumor microtube networks for selective drug transport and augmentation of antitumor effects in orthotopic lung cancer. *Theranostics* 9 (23), 6936–6948. doi:10.7150/thno.37380

Guo, Q., Yan, J., Song, T., Zhong, C., Kuang, J., Mo, Y., et al. (2021). microRNA-130b-3p contained in MSC-derived EVs promotes lung cancer progression by regulating the FOXO3/NFE2L2/TXNRD1 Axis. *Mol. Ther. Oncolytics* 20, 132–146. doi:10.1016/j.omto.2020.09.005

Harris, M. A., Clark, J., Ireland, A., Lomax, J., Ashburner, M., Foulger, R., et al. (2004). The Gene Ontology (GO) database and informatics resource. *Nucleic Acids Res.* 32, D258–D261. doi:10.1093/nar/gkh036

He, L., Luo, L., Zhu, H., Yang, H., Zhang, Y., Wu, H., et al. (2017). FEN1 promotes tumor progression and confers cisplatin resistance in non-small-cell lung cancer. *Mol. Oncol.* 11 (6), 640–654. doi:10.1002/1878-0261.12058

Ho, J. Y., Lu, H. Y., Cheng, H. H., Kuo, Y. C., Lee, Y. A., and Cheng, C. H. (2021). UBE2S activates NF-κB signaling by binding with IκBα and promotes metastasis of lung adenocarcinoma cells. *Cell. Oncol.* 44 (6), 1325–1338. doi:10.1007/s13402-021-00639-4

Karagkouni, D., Paraskevopoulou, M. D., Chatzopoulos, S., Vlachos, I. S., Tastsoglou, S., Kanellos, I., et al. (2018). DIANA-TarBase v8: A decade-long collection of experimentally supported miRNA–gene interactions. *Nucleic Acids Res.* 46 (D1), D239–D245. doi:10.1093/nar/gkx1141

Lan, Q., Liu, P. Y., Haase, J., Bell, J. L., Hüttelmaier, S., and Liu, T. (2019). The critical role of RNA m6A methylation in cancer. *Cancer Res.* 79 (7), 1285–1292. doi:10.1158/0008-5472.CAN-18-2965

Lee, D. D., and Seung, H. S. (1999). Learning the parts of objects by non-negative matrix factorization.Research Support, Non-U.S. Gov't]. *J. Artic.* 401 (6755), 788–791. doi:10.1038/44565

Lee, S. Y., Choi, Y. Y., Choi, J. E., Kim, M. J., Kim, J., Jung, D. K., et al. (2010). Polymorphisms in the caspase genes and the risk of lung cancer. *J. Thorac. Oncol.* 5 (8), 1152–1158. doi:10.1097/JTO.0b013e3181e04543

Li, D., Fu, Z., Dong, C., and Song, Y. (2022). Methyltransferase 3, N6-adenosine-methyltransferase complex catalytic subunit-induced long intergenic non-protein coding RNA 1833 N6-methyladenosine methylation promotes the non-small cell lung cancer progression via regulating heterogeneous nuclear ribonucleoprotein A2/B1 expression. *Bioengineered* 13 (4), 10493–10503. doi:10.1080/21655979.2022.2061305

Li, J., Han, Y., Zhang, H., Qian, Z., Jia, W., Gao, Y., et al. (2019). The m6A demethylase FTO promotes the growth of lung cancer cells by regulating the m6A level of USP7 mRNA. *Biochem. Biophys. Res. Commun.* 512 (3), 479–485. doi:10.1016/j.bbrc.2019.03.093

Li, K., Peng, Z., Gao, S., Wang, Q., Wang, R., Li, X., et al. (2021). M6A associated TSUC7 inhibition contributed to Erlotinib resistance in lung adenocarcinoma through a notch signaling activation dependent way. *J. Exp. Clin. Cancer Res.* 40 (1), 325. doi:10.1186/s13046-021-02137-9

Li, S., Zhao, C., Gao, J., Zhuang, X., Liu, S., Xing, X., et al. (2021). Cyclin G2 reverses immunosuppressive tumor microenvironment and potentiates PD-1 blockade in glioma. *J. Exp. Clin. Cancer Res.* 40 (1), 273. doi:10.1186/s13046-021-02078-3

Li, Y., Xiao, J., Bai, J., Tian, Y., Qu, Y., Chen, X., et al. (2019). Molecular characterization and clinical relevance of m6A regulators across 33 cancer types. *Mol. Cancer* 18 (1), 137. doi:10.1186/s12943-019-1066-3

Li, Z., Weng, H., Su, R., Weng, X., Zuo, Z., Li, C., et al. (2017). FTO plays an oncogenic role in acute myeloid leukemia as a n 6 -Methyladenosine RNA demethylase. *Cancer Cell* 31 (1), 127–141. doi:10.1016/j.ccell.2016.11.017

Liang, L., Cen, H., Huang, J., Qin, A., Xu, W., Wang, S., et al. (2022). The reversion of DNA methylation-induced miRNA silence via biomimetic nanoparticles-mediated gene delivery for efficient lung adenocarcinoma therapy. *Mol. Cancer* 21 (1), 186. doi:10.1186/s12943-022-01651-4

Liberzon, A., Birger, C., Thorvaldsdóttir, H., Ghandi, M., Mesirov, J. P., and Tamayo, P. (2015). The Molecular Signatures Database (MSigDB) hallmark gene set collection. *Cell Syst.* 1 (6), 417–425. doi:10.1016/j.cels.2015.12.004

Listed, N. (1995). Chemotherapy in non-small cell lung cancer: a meta-analysis using updated data on individual patients from 52 randomised clinical trials. Non-small cell lung cancer collaborative group. *Br. Med. J. Clin. Res. ed.)* 311, 899.

Liu, T., Li, C., Jin, L., Li, C., and Wang, L. (2019). The prognostic value of m6A RNA methylation regulators in colon adenocarcinoma. *Med. Sci. Monit.* 25, 9435–9445. doi:10.12659/MSM.920381

Liu, X. S. (2018). Evaluation of immune repertoire inference methods from RNA-seq data. *Nat. Biotechnol.* 36, 1034. doi:10.1038/nbt.4294

Love, M. I., Huber, W., and Anders, S. (2014). Moderated estimation of fold change and dispersion for RNA-seq data with DESeq2. *Genome Biol.* 15 (12), 550. doi:10.1186/s13059-014-0550-8

Lu, X., He, X., Su, J., Wang, J., Liu, X., Xu, K., et al. (2018). EZH2-Mediated epigenetic suppression of GDF15 predicts a poor prognosis and regulates cell proliferation in non-small-cell lung cancer. *Mol. Ther. Nucleic Acids* 12, 309–318. doi:10.1016/j.omtn.2018.05.016

Luo, Y., Deng, X., Que, J., Li, Z., Xie, W., Dai, G., et al. (2022). Cell Trajectory-Related genes of lung adenocarcinoma predict tumor immune microenvironment and prognosis of patients. *Front. Oncol.* 12, 911401. doi:10.3389/fonc.2022.911401

Ma, L., Xue, X., Zhang, X., Yu, K., Xu, X., Tian, X., et al. (2022). The essential roles of m6A RNA modification to stimulate ENO1-dependent glycolysis and tumorigenesis in lung adenocarcinoma. *J. Exp. Clin. Cancer Res.* 41 (1), 36. doi:10.1186/s13046-021-02200-5

Maeser, D., Gruener, R. F., and Huang, R. S. (2021). OncoPredict: an R package for predicting*in vivo* or cancer patient drug response and biomarkers from cell line screening data. *Brief. Bioinform.* 22 (6), bbab260. doi:10.1093/bib/bbab260

McDaniel, K., Hall, C., Sato, K., Lairmore, T., Marzioni, M., Glaser, S., et al. (2016). Lin28 and let-7: roles and regulation in liver diseases. *Am. J. Physiol. Gastrointest. Liver Physiol.* 310 (10), G757–G765. doi:10.1152/ajpgi.00080.2016

Mering, C. V., Huynen, M., Jaeggi, D., Schmidt, S., Bork, P., and Snel, B. (2003). STRING: a database of predicted functional associations between proteins. *Nucleic Acids Res.* 31 (1), 258–261. doi:10.1093/nar/gkg034

Meyer, K. D., and Jaffrey, S. R. (2017). Rethinking m6 a readers, writers, and erasers. *Annu. Rev. Cell Dev. Biol.* 33 (1), 319–342. doi:10.1146/annurev-cellbio-100616-060758

Miller, K. D., Siegel, R. L., Lin, C. C., Mariotto, A. B., Kramer, J. L., Rowland, J. H., et al. (2016). Cancer treatment and survivorship statistics, 2016. *Ca. Cancer J. Clin.* 66 (4), 271–289. doi:10.3322/caac.21349

Obadimu, A., Mead, E., and Agarwal, N. (2019). "Identifying latent toxicfeatures on YouTube using non-negative matrix factorization," in *The ninth international*

Conference on social media technologies, communication, and informatics (Valencia), 1–6.

Oh, J., Kim, J., Byun, J., and Kim, I. (2010). Lin28-let7 modulates radiosensitivity of human cancer cells with activation of K-Ras. *Int. J. Radiat. Oncol. Biol. Phys.* 76 (1), 5–8. doi:10.1016/j.ijrobp.2009.08.028

Oshi, M., Newman, S., Tokumaru, Y., Yan, L., Matsuyama, R., Endo, I., et al. (2020). High G2M pathway score pancreatic cancer is associated with worse survival, particularly after margin-positive (R1 or R2) resection. *Cancers* 12 (10), 2871. doi:10.3390/cancers12102871

Osmani, L., Askin, F., Gabrielson, E., and Li, Q. K. (2018). Current WHO guidelines and the critical role of immunohistochemical markers in the subclassification of non-small cell lung carcinoma (NSCLC): Moving from targeted therapy to immunotherapy. *Semin. Cancer Biol.* 52, 103–109. doi:10.1016/j.semcancer.2017.11.019

Paraskevopoulou, M. D., Vlachos, I. S., Karagkouni, D., Georgakilas, G., Kanellos, I., Vergoulis, T., et al. (2016). DIANA-LncBase v2: Indexing microRNA targets on non-coding transcripts. *Nucleic Acids Res.* 44 (D1), D231–D238. doi:10.1093/nar/gkv1270

Pastushenko, I., Mauri, F., Song, Y., de Cock, F., Meeusen, B., Swedlund, B., et al. (2021). Fat1 deletion promotes hybrid EMT state, tumour stemness and metastasis. *Nature* 589 (7842), 448–455. doi:10.1038/s41586-020-03046-1

Qian, X., Yang, J., Qiu, Q., Li, X., Jiang, C., Li, J., et al. (2021). LCAT3, a novel m6A-regulated long non-coding RNA, plays an oncogenic role in lung cancer via binding with FUBP1 to activate c-MYC. *J. Hematol. Oncol.* 14 (1), 112. doi:10.1186/s13045-021-01123-0

Qin, Y., Du, J., and Fan, C. (2020). Ube2S regulates Wnt/β-catenin signaling and promotes the progression of non-small cell lung cancer. *Int. J. Med. Sci.* 17 (2), 274–279. doi:10.7150/ijms.40243

Queirolo, P., and Spagnolo, F. (2017). Atypical responses in patients with advanced melanoma, lung cancer, renal-cell carcinoma and other solid tumors treated with anti-PD-1 drugs: A systematic review. *Cancer Treat. Rev.* 59, 71–78. doi:10.1016/j.ctrv.2017.07.002

Robin, X., Turck, N., Hainard, A., Tiberti, N., Lisacek, F., Sanchez, J., et al. (2011). PROC: an open-source package for R and S+ to analyze and compare ROC curves. *BMC Bioinforma.* 12 (1), 77. doi:10.1186/1471-2105-12-77

Robinson, D. R., Zylstra, C. R., and Williams, B. O. (2008). Wnt signaling and prostate cancer. *Curr. Drug Targets* 9 (7), 571–580. doi:10.2174/138945008784911831

Ruiz-Cordero, R., and Devine, W. P. (2020). Targeted therapy and checkpoint immunotherapy in lung cancer. *Surg. Pathol. Clin.* 13 (1), 17–33. doi:10.1016/j.path.2019.11.002

Scagliotti, G. V., De Marinis, F., Rinaldi, M., Crinò, L., Gridelli, C., Ricci, S., et al. (2002). Phase III randomized trial comparing three Platinum-Based doublets in advanced non–Small-Cell lung cancer. *J. Clin. Oncol.* 20 (21), 4285–4291. doi:10.1200/JCO.2002.02.068

Schiller, J. H., Harrington, D., Belani, C. P., Langer, C., Sandler, A., Krook, J., et al. (2002). Comparison of four chemotherapy regimens for advanced non-small-cell lung cancer. *N. Engl. J. Med.* 346 (2), 92–98. doi:10.1056/NEJMoa011954

Shannon, P., Markiel, A., Ozier, O., Baliga, N. S., Wang, J. T., Ramage, D., et al. (2003). Cytoscape: A software environment for integrated models of biomolecular interaction networks. *Genome Res.* 13 (11), 2498–2504. doi:10.1101/gr.1239303

Socinski, M. A., Evans, T., Gettinger, S., Hensing, T. A., VanDam, S. L., Ireland, B., et al. (2013). Treatment of stage IV non-small cell lung cancer: Diagnosis and management of lung cancer, 3rd ed: American college of chest physicians evidence-based clinical practice guidelines. *Chest* 143, e341S–e368S. doi:10.1378/chest.12-2361

Steen, C. B., Liu, C. L., Alizadeh, A. A., and Newman, A. M. (2020). Profiling cell type abundance and expression in bulk tissues with CIBERSORTx. *Methods Mol. Biol.* 2117, 135–157. doi:10.1007/978-1-0716-0301-7_7

Subramanian, A., Tamayo, P., Mootha, V. K., Mukherjee, S., Ebert, B. L., Gillette, M. A., et al. (2005). Gene set enrichment analysis: A knowledge-based approach for interpreting genome-wide expression profiles. *Proc. Natl. Acad. Sci. U. S. A.* 102 (43), 15545–15550. doi:10.1073/pnas.0506580102

Travis, W. D., Brambilla, E., and Geisinger, K. R. (2016). Histological grading in lung cancer: One system for all or separate systems for each histological type? *Eur. Respir. J.* 47 (3), 720–723. doi:10.1183/13993003.00035-2016

Walter, W., Sanchez-Cabo, F., and Ricote, M. (2015). GOplot: An R package for visually combining expression data with functional analysis. *Bioinformatics* 31 (17), 2912–2914. doi:10.1093/bioinformatics/btv300

Wang, J., Zhang, C., He, W., and Gou, X. (2020). Effect of m6A RNA methylation regulators on malignant progression and prognosis in renal clear cell carcinoma. *Front. Oncol.* 10, 3. doi:10.3389/fonc.2020.00003

Wen, C., Sun, H., Pan, K., Sun, H., Zhang, Z., Cao, G., et al. (2019). Molecular mechanism exploration of pancreatitis based on miRNA expression profile. *Clin. Lab.* 65 (3). doi:10.7754/Clin.Lab.2018.180807

West, H., McCleod, M., Hussein, M., Morabito, A., Rittmeyer, A., Conter, H. J., et al. (2019). Atezolizumab in combination with carboplatin plus nab-paclitaxel chemotherapy compared with chemotherapy alone as first-line treatment for metastatic non-squamous non-small-cell lung cancer (IMpower130): A multicentre, randomised, open-label, phase 3 trial. *Lancet. Oncol.* 20 (7), 924–937. doi:10.1016/S1470-2045(19)30167-6

Winterbourn, C. C. (2008). Reconciling the chemistry and biology of reactive oxygen species. *Nat. Chem. Biol.* 4 (5), 278–286. doi:10.1038/nchembio.85

Wu, T., Hu, E., Xu, S., Chen, M., Guo, P., Dai, Z., et al. (2021). ClusterProfiler 4.0: A universal enrichment tool for interpreting omics data. *Innovation.* 2 (3), 100141. doi:10.1016/j.xinn.2021.100141

Xia, C., Dong, X., Li, H., Cao, M., Sun, D., He, S., et al. (2022). Cancer statistics in China and United States, 2022: profiles, trends, and determinants. *Chin. Med. J.* 135 (5), 584–590. doi:10.1097/CM9.0000000000002108

Xiang, Y., Laurent, B., Hsu, C., Nachtergaele, S., Lu, Z., Sheng, W., et al. (2017). Corrigendum: RNA m6A methylation regulates the ultraviolet-induced DNA damage response. *Nature* 552 (7685), 430. doi:10.1038/nature24007

Yan, L., Jiao, D., Hu, H., Wang, J., Tang, X., Chen, J., et al. (2017). Identification of lymph node metastasis-related microRNAs in lung adenocarcinoma and analysis of the underlying mechanisms using a bioinformatics approach. *Exp. Biol. Med.* 242 (7), 709–717. doi:10.1177/1535370216677353

Yan, M., Yin, X., Zhang, L., Cui, Y., and Ma, X. (2022). High expression of HOXB3 predicts poor prognosis and correlates with tumor immunity in lung adenocarcinoma. *Mol. Biol. Rep.* 49 (4), 2607–2618. doi:10.1007/s11033-021-07064-8

Yang, N., Kaur, S., Volinia, S., Greshock, J., Lassus, H., Hasegawa, K., et al. (2008). MicroRNA microarray IdentifiesLet-7i as a novel biomarker and therapeutic target in human epithelial ovarian cancer. *Cancer Res.* 68 (24), 10307–10314. doi:10.1158/0008-5472.CAN-08-1954

Yang, W., Soares, J., Greninger, P., Edelman, E. J., Lightfoot, H., Forbes, S., et al. (2012). Genomics of drug sensitivity in cancer (GDSC): A resource for therapeutic biomarker discovery in cancer cells. *Nucleic Acids Res.* 41 (D1), D955–D961. doi:10.1093/nar/gks1111

Yang, Y., Li, H., Liu, Y., Chi, C., Ni, J., and Lin, X. (2019). MiR-4319 hinders YAP expression to restrain non-small cell lung cancer growth through regulation of LIN28-mediated RFX5 stability. *Biomed. Pharmacother.* 115, 108956. doi:10.1016/j.biopha.2019.108956

Yao, H., Lu, F., and Shao, Y. (2020). The E2F family as potential biomarkers and therapeutic targets in colon cancer. *PeerJ* 8, e8562. doi:10.7717/peerj.8562

Zhang, W., Tang, Y., Guo, Y., Kong, Y., Shi, F., Sheng, C., et al. (2022). Favorable immune checkpoint inhibitor outcome of patients with melanoma and NSCLC harboring FAT1 mutations. *NPJ Precis. Oncol.* 6 (1), 46. doi:10.1038/s41698-022-00292-6

Zhang, Z., Zhang, C., Luo, Y., Wu, P., Zhang, G., Zeng, Q., et al. (2021a). M6A regulator expression profile predicts the prognosis, benefit of adjuvant chemotherapy, and response to anti-PD-1 immunotherapy in patients with small-cell lung cancer. *BMC Med.* 19 (1), 284. doi:10.1186/s12916-021-02148-5

Zhang, Z., Zhang, C., Yang, Z., Zhang, G., Wu, P., Luo, Y., et al. (2021b). M6A regulators as predictive biomarkers for chemotherapy benefit and potential therapeutic targets for overcoming chemotherapy resistance in small-cell lung cancer. *J. Hematol. Oncol.* 14 (1), 190. doi:10.1186/s13045-021-01173-4

Zushi, Y. (2021). NMF-Based spectral deconvolution with a web platform GC mixture touch. *ACS Omega* 6 (4), 2742–2748. doi:10.1021/acsomega.0c04982